Lateral torsional buckling of glulam beams

Janusch Töpler, Institute of Structural Design, University of Stuttgart, Germany

Ulrike Kuhlmann, Institute of Structural Design, University of Stuttgart, Germany

Keywords: Stability, lateral torsional buckling, glulam, imperfections, experimental results, numerical modelling

1 Introduction

For the design verification of imperfection-sensitive glulam beams loaded by bending (and axial) force, the lateral torsional buckling (LTB) behaviour is decisive, see Figure 1. The standard design formulae for LTB in EN 1995-1-1 (2004) and prEN 1995-1-1 (2023), the k_m method, were derived analytically. Current drawbacks of the analytical derivation of the k_m method are: (i) the assumption of pure bow imperfections based on very few measurements (*Brüninghoff*, 1973), whose values are inconsistent with extensive measurement results of glulam columns (*Ehlbeck* & *Blaß*, 1987) and do not account for relevant twist imperfections (*Töpler* & *Kuhlmann*, 2022b); (ii) very few experimental data available for validation of the design models (*Brüninghoff*, 1973), (*Larsen*, 1977).

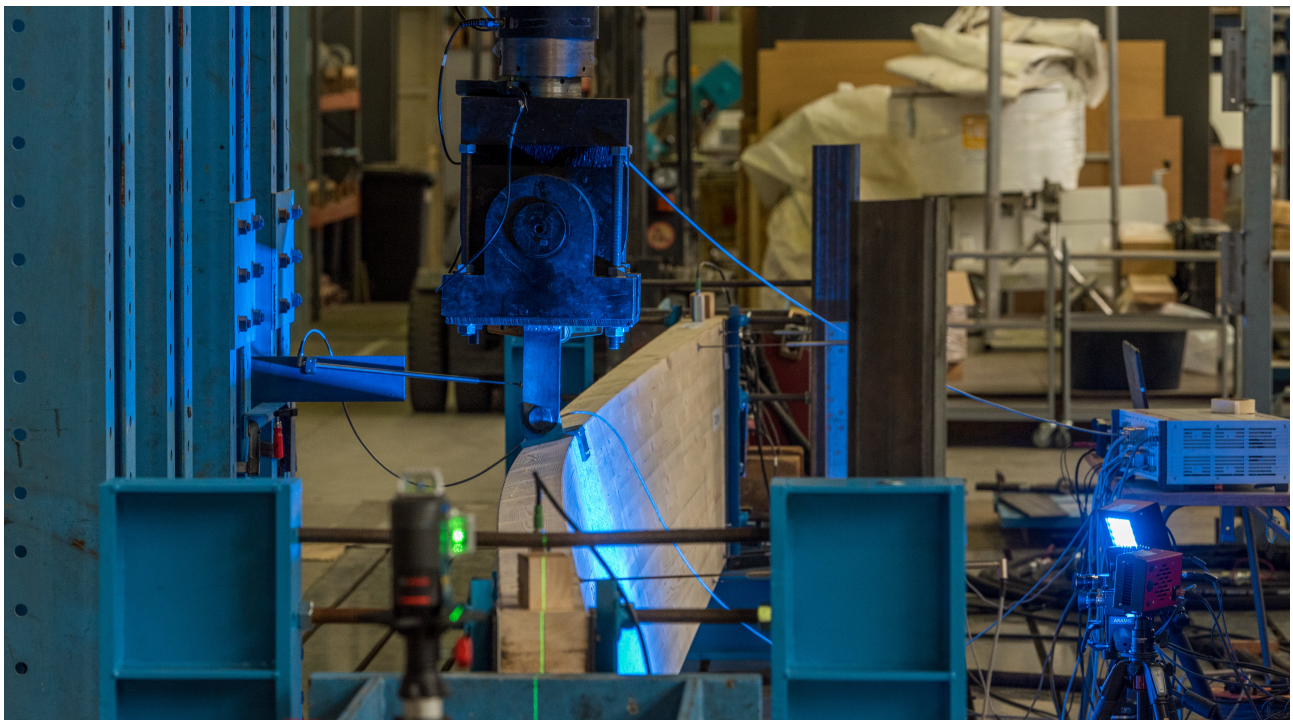

Figure 1. LTB test T02; glulam beam with dimensions 8000 x 720 x 120 mm³ shortly before failure.

This is different from the derivation of the k_c method for in-plane buckling design of timber columns, where extensive numerical investigations with scattering basic variables (material properties and geometric imperfections) were performed (*Ehlbeck* & *Blaß*, 1987) and the results were validated by experimental tests.
A re-evaluation of the design formulae for LTB in EN 1995-1-1 (2004) was therefore considered necessary and was carried out by the authors.

This paper presents the results of 19 full-scale LTB tests on glulam beams carried out by the Institute of Structural Design at the FMPA Cottbus in spring 2023 within a research project (*Kuhlmann* & *Töpler*, 2021-2023), see Figure 1. A numerical model was verified and validated with the test results according to the FE guidelines, see Töpler & Kuhlmann (2022a). The model was used to perform Monte Carlo simulations on glulam beams at risk of LTB with scattering input values, including geometrical imperfections. Due to the test results, it was necessary to additionally investigate the influence of structural imperfections (scattering material properties) and shear failure. The findings are compared with current design rules.
The objectives are to clarify the influence of scattering geometrical and structural imperfections on the LTB of glulam beams, to propose values for equivalent imperfections, to evaluate the design formulae for LTB and to assess the influence of shear from torsion.

2 State of the art

The load-bearing behaviour of imperfection-sensitive timber beams is characterised by geometrically and materially non-linear behaviour. Relevant member failure modes for straight beams with constant cross-section loaded by $M_{y,I}$ are tensile failure due to bending moments $M_{y,II}$ and $M_{z,II}$ and shear failure due to combined shear forces V_z and torsional moments $M_{x,II}$. Besides the effects of geometry, type of loading, boundary conditions and resulting eigenmodes, the geometrically non-linear behaviour is influenced by stiffnesses E and G and imperfections. The materially non-linear behaviour only needs to be taken into account for compression parallel to the grain according to current knowledge.

For the bending resistance of glulam beams prone to LTB, EN 1995-1-1 (2004) and prEN 1995-1-1 (2023) provide two design approaches, the effective length method (ELM) and design verification based on the calculation of internal forces according to second order theory (T2O).
For the ELM, the formula for determination of k_m in EN 1995-1-1 (2004) is based on curve fitting to the exact solution of the differential equations of the LTB phenomenon, the T2O formulae (*Heimeshoff*, 1986). For the fitting process, pure bow imperfections $e_y = L/288$ and $L/577$ were assumed. Within prEN 1995-1-1 (2023), a reformulation of k_m according to the Ayrton-Perry formulation is proposed, which can be derived from the T2O solution under certain assumptions, as illustrated by *Wilden* et al. (2023). The limits $\lambda_{m,rel} = 0.75$ and 0.55 in EN 1995-1-1 (2004) and prEN 1995-1-1 (2023) are pragmatic

estimates of the points where the influence of LTB can be neglected in building practice. T2O provides accurate solutions for the equivalent beam assuming linear elastic material behaviour. The linear elastic material behaviour is thus also implied in k_{m}. As the tensile strength of softwood glulam in bending f_{m} is about the same as the proportionality limit for compression $f_{\mathrm{c,0,lin}}$, this assumption usually holds for pure bending, for strengths see e.g. Table 4.

The assumption of pure bow imperfections for LTB of timber beams and its values (ELM: *L*/288 and *L*/577, see *Heimeshoff* (1986); T2O: *L*/400, see EN 1995-1-1 (2004)) are based on measurements on one building (*Brüninghoff*, 1973). The differences with the extensive measurements on glulam columns by *Ehlbeck* & *Blaß* (1987), which resulted in a 95% quantile value of the bow imperfection of about *L*/1100, might be explained by different causes of the imperfections, such as manufacturing for unbraced columns and alignment for braced beams. Recent measurements by *Töpler* & *Kuhlmann* (2022b) yielded smaller bow imperfections e_{y}, but highlighted the importance of twist imperfections at supports $e_{\vartheta,\mathrm{supp}}$ and midspan $e_{\vartheta,\mathrm{mid}}$. 95% quantile values of measured imperfections were:

- bow imperfections: $e_{\mathrm{y,95}} = \frac{L}{1180}$ [mm]
- twist imperfections at midspan: $e_{\vartheta,\mathrm{mid,95}} = \frac{L}{1590H}$ [-]
- twist imperfections at supports with high tolerances: $e_{\vartheta,\mathrm{supp,95}} = \frac{1}{100}$ [-]
- twist imperfections at supports with low tolerances: $e_{\vartheta,\mathrm{supp,95}} = \frac{1}{170}$ [-]

Where high tolerances refer to fork bearings by means of concrete pockets or similar and low tolerances refer to fork bearings by means of lateral timber members or similar. These measurement results are incorporated in the imperfection assumptions in prEN 1995-1-1 (2023). A formulation of simplified equivalent imperfections is still pending.

The effects of structural imperfections caused by material scattering on the LTB design of glulam beams are generally neglected, which is justified by the homogenisation effect due to the large number of lamellae. This is in contrast to glulam columns, where scattering of the elastic moduli of different lamellae can significantly influence the position of the shear centre (*Ehlbeck* & *Blaß*, 1987).

The design formulae for LTB in EN 1995-1-1 (2004) were validated mostly with small scale tests on solid timber (*Larsen*, 1977). Very few results of full scale tests on glulam have been published (*Brüninghoff*, 1973), (*Wilden* et al., 2023).

For the design verification of the shear resistance of timber beams prone to LTB, no information is given in EN 1995-1-1 (2004) on the consideration of the torsional moment. A slenderness criterion is mentioned in the National Annex DIN EN 1995-1-1/NA (2013). If satisfied, shear stress components from torsion may be neglected. prEN 1995-1-1 (2023) gives formulae for determining the torsional moments at the supports $M_{\mathrm{x,II}}$.

3 Experiments

3.1 General

Lateral torsional buckling tests on 19 glulam beams made of GL 24h according to EN 14080 (2013) were conducted in order to experimentally investigate the load-deformation behaviour and serve as validation for a finite element (FE) model. The slenderness was varied over the beam length and height and the ratio of the normal force to the bending moment, see Table 1. As the focus of this article is on pure bending, the results of the tests with axial force are not reported here, but will be in *Töpler* (2024). All beams were of constant rectangular cross-section. The load introduction and support areas were reinforced with pre-drilled, fully threaded screws.

Table 1. Test program for lateral torsional buckling of glulam GL 24h beams.

Series number	Number of specimens	Length [mm]	Height x Width [mm²]	$\lambda_{m,rel}$*	Axial force [kN]
T01- T03	3	8000	720 x 120	1.04	0
T04- T05	2	8000	600 x 120	0.94	0
T06- T07	2	8000	600 x 120	0.94	25
T08- T09	2	8000	600 x 120	0.94	50
T10- T11	2	8000	600 x 120	0.94	75
T12- T13	2	6000	480 x 120	0.74	0
T14- T15	2	6000	480 x 120	0.74	35
T16- T17	2	6000	480 x 120	0.74	70
T18- T19	2	6000	480 x 120	0.74	105

* Calculated with characteristic material values, taking into account an increase of $E_{0,05}G_{0,05}$ by a factor of 1.4 according to DIN EN 1995-1-1/NA (2013).

For validation of the FE model in Section 4, the geometrical imperfections were determined in preceding measurements with the optical measurement system ARAMIS Adjustable 12M. Cross-sectional dimensions, weight, moisture content, knots and finger joints were documented. Mean density and moisture content of all test specimens were 444 kg/m³ and 10.4%.

For each test specimen, see Table 1, the elastic moduli for edgewise and flatwise bending $E_{0,y/z}$ and the shear modulus G_0 were determined in elastic bending and torsion tests with test setups, speed and direction of loading mirroring to the following LTB tests. The summarised results are displayed in Table 2. Since the values in Table 2 were used for the validation of the FE model in Section 4, they were determined iteratively with a similar FE model. Mean values $E_{0,mean}$ and $G_{0,mean}$ were 12,100 and 747 N/mm². $E_{0,y}$ and $E_{0,z}$ for edgewise and flatwise bending were almost identical on average with maximum deviations of 12% and thus could be combined into E_0.

The stress-strain curves for compression parallel to the grain were determined in compression tests on 8 test specimens from 4 lamellae according to EN 408 (2010). Resulting mean compression strength, proportionality limit and plastic strain when reaching the compression strength were $f_{c,0}$ = 43.2 N/mm², $f_{c,0,lin} = 0.71 \cdot f_{c,0}$ and $\epsilon_{c,0,pl} = 0.45 \cdot \epsilon_{c,0,el}$ for a slightly higher density of 504 kg/m³.

Table 2. Results of elastic bending and torsion tests.

	$E_{0,y}$ [N/mm²]	$E_{0,z}$ [N/mm²]	$E_{0,y}/E_{0,z}$	E_0 [N/mm²]	G_0 [N/mm²]
Mean	12,139	12,050	1.006	12,095	747
COV	0.0830	0.0503	0.0466	0.0644	0.0616
Min	10,906	11,223	0.940	11,081	625
Max	14,734	13,152	1.120	13,943	812

3.2 Lateral torsional buckling tests

3.2.1 Test setup and execution

The LTB experiments were conducted as 3-point bending tests, see Figure 2. Vertical loading was applied at the upper edge in midspan with a horizontal eccentricity perpendicular to the beam axis of 8 mm for a planned buckling in a defined direction. The distance between the upper edge of the beam and the axis of rotation of the load (screw axis) resulted in an additional vertical eccentricity of 53 mm, see Figure 3. To ensure a vertical loading when the beam deformed horizontally, the upper bearing of the vertical cylinder could be automatically moved horizontally by up to 220 mm. For limiting dynamic behaviour of the test set-up in the event of sudden lateral deformations of the timber beams, the vertical cylinder was inclined by 10 to 20 mm over its 2210 mm length, acting in the same direction as the horizontal load eccentricity. The supports were constructed as ideal fork bearings. The measurement of the complex deformation behaviour at midspan was conducted with the optical measuring system ARAMIS Adjustable 12M.

Beams with and without axial force were tested, see Table 1. Axial forces were applied first and force-controlled up to the levels given in Table 1. Vertical forces were applied displacement-controlled at a rate of 4 to 5 mm/min, which resulted in a failure in about 10 to 20 minutes.

Figure 2. LTB test setup.

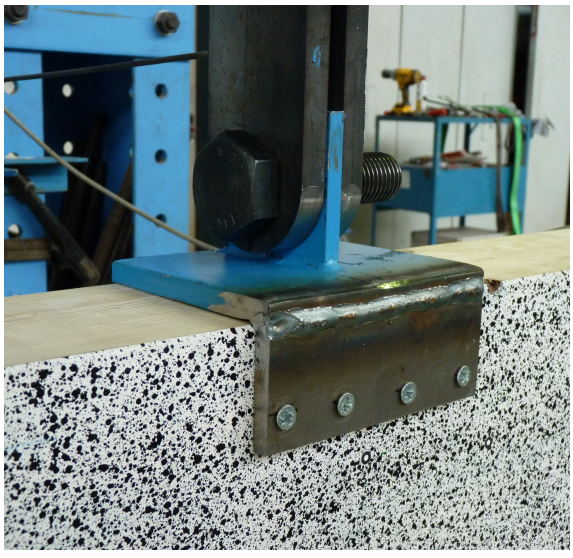

Figure 3. Vertical load introduction for LTB.

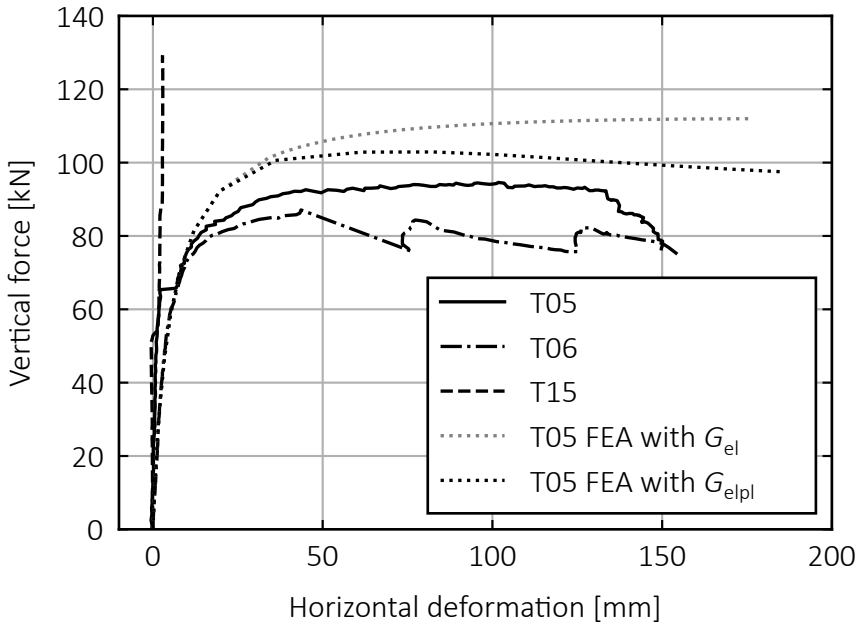

Figure 4. Vertical force and horizontal deformation of the beam axis at midspan of T05, T06 and T15, experimental results; numerical recalculation of T05 for model validation (FEA).

3.2.2 Results and evaluation

Typical load-deformation curves with the horizontal deformation of the beam axis at midspan and the vertical cylinder force are given in Figure 4 for beams T05, T06 and T15. The curves of 16 out of 19 tests were non-linear from the beginning, see T05 and T06. After about 80% of the load-bearing capacity was reached, large horizontal deformations occurred, see Figure 1, leading to a plateau of the load-deformation curve. In some cases local failures caused load drops, see T06. The tests were stopped when either a brittle member failure occurred or the load dropped below 80% of the maximum load-bearing capacity. In 3 cases the beams failed in uniaxial bending without showing LTB behaviour, see T15 in Figure 4. The applied horizontal eccentricity of 8 mm and the inclination of the vertical cylinder were not sufficient to overcome the effects of geometrical and structural imperfections, as well as friction in the supports and load application. The measured geometric bow imperfections ranged from 1.4 to 6.7 mm in the opposite direction to the load eccentricity and therefore cannot fully explain this behaviour. This indicates that there were additionally significant structural imperfections. This effect is further investigated in Section 4.3.

The experimentally determined normalised load-bearing capacities k_{m} of all beams (exp) are plotted over the relative slenderness ratio $\lambda_{\mathrm{m,rel}}$ in Figure 5. $\lambda_{\mathrm{m,rel}}$ was always computed with characteristic material values utilising the increase of $1.4 \cdot E_{0,05} G_{0,05}$ for glulam. k_{m} was calculated by dividing the experimental resistances by the nominal characteristic resistances $f_{\mathrm{m,k}} W_{\mathrm{y}}$. Results of the ELM are given for characteristic strengths. For the load-bearing capacity in bending of a 480 x 120 mm² cross-section according to T2O, three curves are given with characteristic, mean and 95% quantile values of the strengths

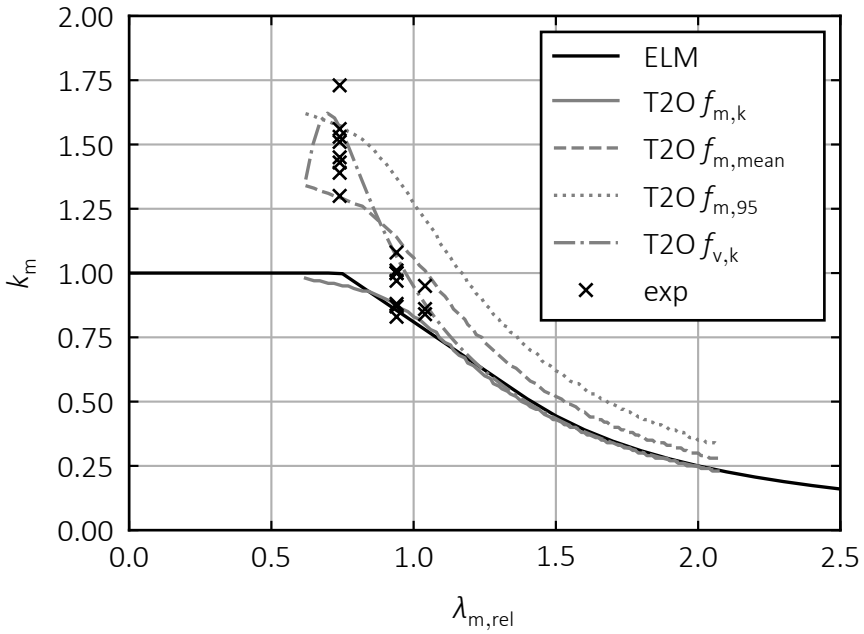

Figure 5. Experimentally determined, normalised resistances k_m in comparison with bending resistances using ELM and T2O and shear resistances using T2O according to EN 1995-1-1 (2004).

and stiffnesses, assuming values from EN 14080 (2013) and $f_{m,mean}$ = 33.0 N/mm², $f_{m,95}$ = 40.0 N/mm², $E_{0,95}$ = 13800 N/mm² and $G_{0,95}$ = 780 N/mm². Additionally, the curve of the characteristic load-bearing capacity of a 480 x 120 mm² cross-section in shear is given. For ELM and T2O no axial forces were considered. The diagram illustrates that the LTB bending design for service class 1 according to EN 1995-1-1 (2004) is on the safe side. Only the experimental results of the beams T08 to T11 with significant axial forces are of the same magnitude as the calculated characteristic resistances without axial forces. It is noteworthy that for the larger slendernesses the experimentally determined load-bearing capacities are about 10% below and for the small slenderness about 15% above the mean values of the bending resistances according to T2O. The experimental results rather follow the shape of the curve of the characteristic shear resistance. This will be further discussed, as it is based on a change of the failure behaviour and the significant influence of a reduced shear stiffness.

Three failure modes were observed, tensile failure due to bending, shear failure and compression failure, see Figures 6 and 7. In 14 out of 18 tests (not documented for T01), loud cracking was audible above 70% of the maximum load-bearing capacity, indicating a significant local failure and leading to a flattening of the load-deformation curve. Only in 4 cases this was visible in the form of local shear or tensile cracks, see Table 3. In 12 tests, an abrupt brittle member failure occurred. The remaining 7 tests were aborted when the load dropped below 80% of the maximum load-bearing capacity. In 10 cases, member failure occurred in tension and in 2 cases in shear, expressed as a diagonal crack from the loading area to one support that partially cut through the cross-section completely, see Figures 6 and 7. Member failure in tension was always accompanied by transverse

Table 3. Visible failure behaviour before and at the end of the experiments.

Series number	Member failure	Localised failure at the end			Localised failure before the end
		Tensile	Shear	Compression	
T01	-	-	x	*	-
T02	-	-	x	x	-
T03	Shear	-	x	x	-
T04	Tensile	x	x	x	-
T05	-	x	x	x	-
T06	-	x	x	x	Tensile & Shear
T07	Tensile	x	x	-	-
T08	Tensile	x	x	x	Tensile
T09	Shear	-	x	x	Shear
T10	-	-	x	x	-
T11	-	-	x	x	-
T12	Tensile	x	-	-	-
T13	Tensile	x	-	x	-
T14	Tensile	x	-	x	-
T15	Tensile	x	-	-	-
T16	Tensile	x	-	-	-
T17	Tensile	x	-	x	-
T18	Tensile	x	-	x	-
T19	-	x	x	x	Tensile & Shear

* Could not bet documented.

tensile failure, see Figure 6. Minor local buckling of the wood fibres under compression parallel to the grain was observed in 14 cases at the load application area. Table 3 shows that the slender beams T01 to T03 failed exclusively in shear, while the stocky beams T12 to T19 usually failed in tension. For T04 to T11 both failure mechanisms were present. As torsional moments increase with increasing slenderness, it can be concluded that the shear failure was mainly caused by torsion. This failure was not expected to this extend, as characteristic shear resistances according to T2O are 10 to 20% higher than bending resistances, see Figure 5. The loud cracking, which was followed by a flattening of the load-deformation curve, indicates that this local shear failure significantly influenced the load-bearing capacity, reducing it by 10 to 20%, see Figure 5. This is supported by the numerical results, see Section 4.4.

Figure 6. Tensile failure of T04.

Figure 7. Diagonal shear failure of T09.

4 Numerical simulations

4.1 General

The first objective of the numerical simulations was to investigate the influence of scattering geometrical imperfections and scattering material stiffnesses across the width of the glulam lamellae (structural imperfections) on the load-bearing behaviour of imperfection-sensitive glulam beams using a verified and validated FE model.
The occurrence of a second member failure mechanism in the tests, shear, also made it necessary to provide a first estimate of the proportion of shear failure and the proportion of bending failure that govern the LTB resistance of glulam beams. For this assessment, a modelling approach with scattering material properties based on the *Karlsruher Rechenmodell* (*Blaß* et al., 2008) was developed.

The numerical calculations were conducted with a FE model in Abaqus/CAE 2023. 20-node quadratic brick elements C3D20R were used. A detailed description of the model will be given in *Töpler* (2024).
Since Abaqus internal material models do not allow for pure uniaxial plasticising under compression parallel to the grain or independent shear plasticising, a user-defined material model was developed in the UMAT subroutine. For tension parallel to the grain, a linear elastic material behaviour was implemented with softening to a minimum residual strength when the tensile strength is exceeded. This corresponds with the failure behaviour in the *Karlsruher Rechenmodell* (*Blaß* et al., 2008). For compression parallel to the grain, plasticising was considered along an ellipse according to *Töpler* & *Kuhlmann* (2022c). For shear, a bilinear material behaviour in all 3 material planes was assumed. A shear interaction was considered as well but had no significant effect.
The initial material values are given in Table 4, which are reasonable mean values for GL 24h. $E_{R/T}$ was selected to 300 N/mm² in accordance with EN 14080 (2013) and all Poisson's ratios were set to 0.3.

Table 4. Material values for numerical modelling.

	Elastic modulus [N/mm²]	Proportionality limit [x Strength]	Strength [N/mm²]	Plastic strain at strength [-]	Plastic modulus [N/mm²]
Tension in L	11,500	-	33.0	-	-
Compression in L	11,500	0.75	40.0	0.40	50
Shear in LR	650	0.30	5.3	-	975
Shear in LT	650	0.30	5.3	-	975
Shear in RT	100	0.55	1.6	-	32.5

L = longitudinal, R = radial, T = tangential direction.

Plastic strains are determined with the plastic moduli (for compression with consideration of the elliptical inclination). Moduli of elasticity and shear in the LR and LT planes were picked according to EN 14080 (2013), rolling shear properties according to *Aicher* & *Dill-Langer* (2000), *Dahl* & *Malo* (2009), *Ehrhart* & *Brandner* (2018), proportionality limit in compression according to own tests in Section 3, compression and tensile

strengths according to *Glos* (1978), *Schilling* et al. (2021), shear strengths in the LR/LT planes according to *Glos* & *Denzler* (2004), *Spengler* (1986), plastic compression strain according to own tests in Section 3 and *Glos* (1978) and plastic stiffness components for shear according to *Dahl* & *Malo* (2009). For the plastic component in compression a reasonable value resulting in a minimum slope of the stress-strain curve was chosen. The low proportionality limit for shear in the LR and LT planes needs to be highlighted. It has a significant influence on the load-deformation behaviour of LTB and, in the opinion of the authors, represents the point of the first occurrence of a significant local shear failure in the tests that led to a flattening of the load-deformation curve, see Section 3.2.2. Numerically determined shear stresses at the time of the first occurrence of this audible significant local failure ranged from 1.1 to 2.6 N/mm². Therefore, a mean value of 1.6 N/mm² $= 0.3 \cdot 5.3$ N/mm² was set as the proportionality limit.

4.2 Geometrical imperfections

In the parameter study, scattering geometrical imperfections with random values were assumed based on distribution functions obtained from measurements, see Section 2 and *Töpler* & *Kuhlmann* (2022b). As a reasonable approximation of the frequency distributions of the measured imperfections, normal distributions with a mean of zero and the following properties were utilised (μ;σ;limit):

- bow imperfections: $\frac{e_y}{L}$: N(0;0.0004272;0.0015) [mm/mm]
- twist imperfections at midspan: $\frac{e_{\vartheta,\text{mid}}H}{L}$: N(0;0.0002667;0.0012) [mm/mm]
- twist imperfections at supports: $e_{\vartheta,\text{supp}}$: N(0;0.004790;0.02) [-]

To be on the safe side, fork bearings with high tolerances were chosen for the values of the twist imperfections. No significant correlations supported by causality were found between the different imperfections, except for the twist imperfections at both supports. Twist imperfections at the supports are mainly influenced by the placement of a beam in the fork bearings (rigid body rotation of the entire beam), the twisting of the beam along its length due to manufacturing, transport, etc., and the alignment of the beam at the supports (twist of the cross-section at both supports against each other). To represent these effects in the model, first the twist at one support $e_{\vartheta,\text{supp},0}$ was determined from the above distribution, then the basic value of the twist at the other support $e_{\vartheta,\text{supp,L}}$ was determined by linear regression, and finally an error term was added to this value, see Equation 1.

$$e_{\vartheta,\text{supp,L}} = 0.5272 \cdot e_{\vartheta,\text{supp},0} + e \qquad \text{with} \quad e\text{:} \quad \text{N}(0; 0.004070; -) \tag{1}$$

4.3 Structural imperfections and scattering material properties

For the assessment of the proportion of shear and bending failure, scattering material properties according to the *Karlsruher Rechenmodell*, see *Blaß* et al. (2008) and *Frese* (2016), were implemented in the FE model. The material data were generated before the FE analysis with a Python script. Visual grading VIS-2 according to *Blaß* et al. (2008) was chosen, as it can be used to sort boards for GL 24h. The model for scattering shear strengths of boards is based on *Brüninghoff* & *Klapp* (2005). Thereby, shear strengths are assigned to each board independently using a distribution function. Since the dry densities of the boards are already defined by the *Karlsruher Rechenmodell*, a low correlation of dry density and shear strength according to *Glos* & *Denzler* (2004) was taken into account. The scattering shear strength of each board was computed, as

$$f_{v,LR/LT} = 0.00135 \cdot \rho_0 + 4.75 + e \qquad \text{with} \quad e\text{:} \quad N(0; 0.90; -) \tag{2}$$

where $f_{v,LR/LT}$ is the shear strength in the LR and LT planes in N/mm² and ρ_0 is the dry density in kg/m³. The resulting mean and characteristic shear strengths for VIS-2 are about 5.3 and 3.8 N/mm².

Scattering of elastic moduli across the width of the boards, which is relevant to LTB as it causes structural imperfections in the direction of the weak beam axis, is not considered in models such as the *Karlsruher Rechenmodell*. Local defects like knots have a significant effect on the strength of boards and whole beams, but only a minor effect on the stiffness of beams. In contrast, the distribution of density and the microfibril angle across the board cross-section, which depend on the location of the pith, have a significant effect on the elastic modulus (*Johansson*, 2003). For a pragmatic estimate of this influence, the relationship between pith distance and the elastic modulus, see Equation 3, given by *Dahlblom* et al. (1996), and the position of the piths in the boards of the LTB test specimen were utilised to evaluate the ratio of the elastic moduli of the left and right halves of the boards to their mean elastic moduli.

$$E_0 = 9700 + 100 \cdot r \tag{3}$$

where E_0 is the elastic modulus parallel to the grain in N/mm² and r is the distance to the pith in mm. The determined standard deviation and mean of the ratio of the elastic moduli of the left and right halves of the boards to the mean elastic modulus of the boards were 0.037 and 0.00. For the shear center of a board, this means that at the value of the standard deviation, it will move 0.12 x the width of the board away from the centre of the board. It is therefore plausible that multiple eccentrically located piths could cause significant structural imperfections in glulam beams. For the parameter study, a scattering deviation of the elastic moduli of the left and right halves of the boards from the mean elastic modulus of the boards was assumed based on a normal distribution with μ = 0.00 and σ = 0.05 (constant over the entire board length).

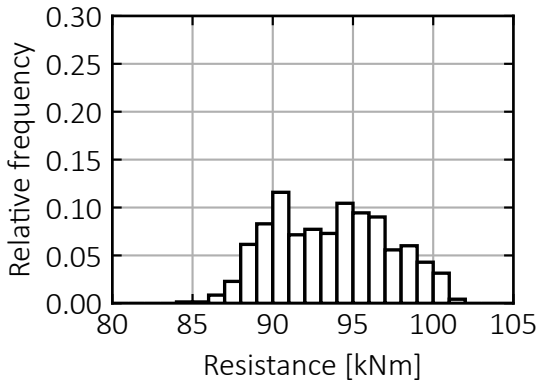

Figure 8. Histogram of the LTB resistances of a beam of L x H x W = 8100 x 600 x 120 mm³ with scattering of geometrical imperfections; 700 computations.

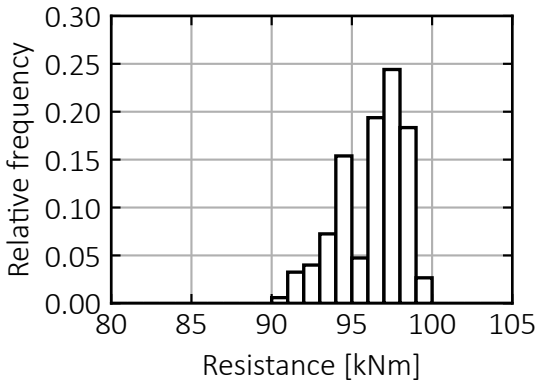

Figure 9. Histogram of the LTB resistances of a beam of L x H x W = 8100 x 600 x 120 mm³ with scattering of structural imperfections; 700 computations.

Both the longitudinal stress distribution in biaxial bending and the shear stress distribution due to torsion indicate a positive size effect on both strengths, as both strengths are determined from tests with a constant stress distribution across the cross-sectional width. These size effects are neglected in the described modelling approach.

4.4 Model verification and validation

The presented FE models were *verified* and *validated* according to the FE guidelines (Töpler & Kuhlmann, 2022a). As part of the verification, a sensitivity analysis was carried out for a single span beam with length x height x width = 8100 x 600 x 120 mm³, basic material values according to Table 4, under a constant bending load $M_{y,l}$ with, (i) scattering of geometrical imperfections according to Section 4.2, and (ii) scattering of elastic moduli across the board width according to Section 4.3. 700 calculations were performed for each. The resistance histograms are displayed in Figures 8 and 9. Structural imperfections have a smaller but still significant effect on the resistances.
For the *validation*, each LTB test was recalculated with the FE model using the measured values for cross-sectional dimensions and elastic and shear moduli, see Section 3. As an example, Figure 4 compares the experimentally and the numerically determined load-deformation curves for T05 (with, G_{elpl}, and without consideration of the plastic behaviour in shear, G_{el}). In this case, the difference between the load-bearing capacity with and without shear plasticising is approximately 10%, which corresponds with the difference between the T2O and the test results, see explanations to Figure 5. The numerical models with shear plasticising generally yield more accurate results than the models without shear plasticising, with a slight overestimation of the load-bearing capacities. Neglecting the three tests in which no LTB occurred, the maximum and mean deviations of the experimentally and the numerically determined load-bearing capacities were 13 and 1.8%, respectively. For the 720 mm high beams, shear failure occurred before bending failure in the FE model, as in the LTB tests. For the stockier beams, bending failure was dominant in the FE analyses.

4.5 Parameter study

Single span beams under a constant bending load $M_{y,l}$ were examined. The first part of the study investigated the influence of imperfections. A cross-section of height x width = 600 x 120 mm² was selected as it was expected to be rather unfavourable due to the low number of lamellae (high structural imperfections), but still prone to LTB. The length was varied in 6 steps between 3000 and 11,400 mm. Two sets of 200 numerical computations each per length were performed, with: (i) scattering of geometrical imperfections and (ii) scattering of geometrical imperfections combined with scattering of elastic moduli across the board width. Deviating from Table 4, characteristic strengths $f_{m,k} = f_{c,0,k}$ = 24.0 N/mm², $f_{v,LR/LT,k}$ = 3.8 N/mm², $f_{v,RT,k}$ = 1.2 N/mm² and mean stiffnesses $E_{0,mean}$ = 11,500 N/mm², $G_{0,mean}$ = 650 N/mm² for GL 24h according to EN 14080 (2013) and *Glos* & *Denzler* (2004) were used for comparability with the design rules in EN 1995-1-1 (2004).

The second part of the study investigated the effect of shear failure on the LTB resistance. A cross-section of length x height x width = 8100 x 720 x 120 mm³ was selected in accordance with the LTB tests where shear failure most likely occurred. Scattering of geometrical imperfections combined with scattering of elastic moduli across the board width, scattering of shear strengths and the *Karlsruher Rechenmodell* for scattering bending strengths were applied. Deviating from Table 4, f_m, $f_{c,0}$, $f_{v,LR/LT}$ and E_0 were generated as described in Section 4.3.

The results of (i) are illustrated in Figure 10. The normalised, scattering numerical results are presented with violin plots supplemented by 5% quantile values (circles), mean values (lower horizontal lines) and 95% quantile values (upper horizontal lines). Additionally, the normalised, characteristic load-bearing capacities of the ELM according to EN 1995-1-1 (2004) and prEN 1995-1-1 (2023) are given. The 5% quantile values of the numerical results follow the typical shape of a LTB curve, where the 95% quantile values follow the cross-sectional resistance and the critical LTB resistance (crit), given by $(\lambda^2_{m,rel})^{-1}$. The scatter of the numerical results clearly demonstrates the influence of imperfections in the range of medium slendernesses between 0.7 and 1.1, while the influence of stiffness and strength is relevant for higher respectively lower slendernesses.

The results of (ii) are similar to (i). In the context of 4 different scattering geometrical imperfections, the bow imperfection, the twist imperfection at midspan and the twist imperfections at both supports, the influence of structural imperfections no longer seems to be significant in the overall results. However, the LTB load-bearing capacities of individual beams can be affected by structural imperfections, see Figure 9.

The results of the second part of the parameter study, which is intended to provide an initial assessment of the proportions of shear and bending failure for LTB, are presented in Figure 11. 13 out of the 200 beams failed in shear in the numerical analysis, while covering a similar range of resistances as bending failure. The 5% quantile values and mean values of the resistance are not significantly influenced by the shear failure.

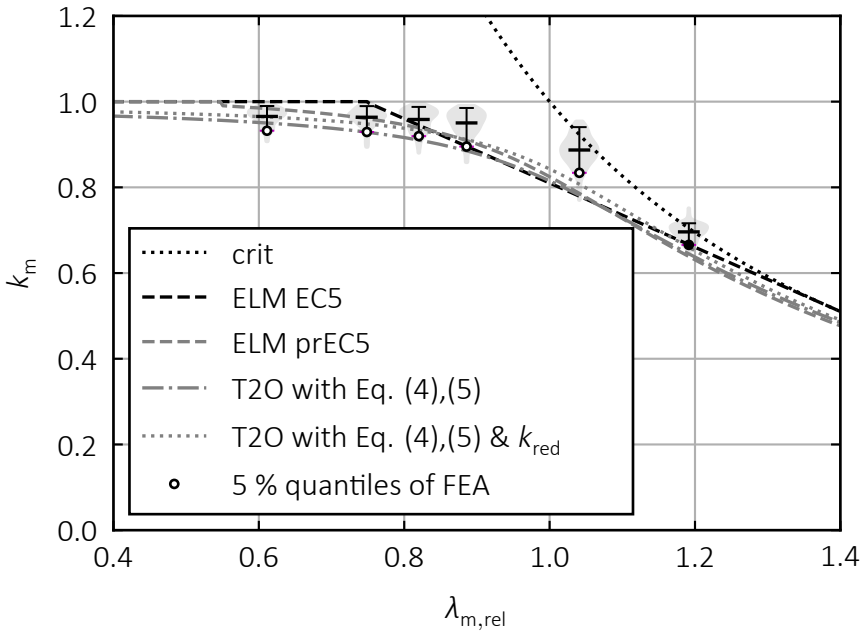

Figure 10. Normalised characteristic load-bearing capacities k_m of 200 FE analyses each at 6 different slendernesses for scattering of geometrical imperfections, (i); compared with critical LTB resistances (crit); bending resistances of ELM according to EN 1995-1-1 (2004) and prEN 1995-1-1 (2023); and bending resistances according to T2O with proposed reduced imperfections, Equations 4 and 5, with and without consideration of k_{red}.

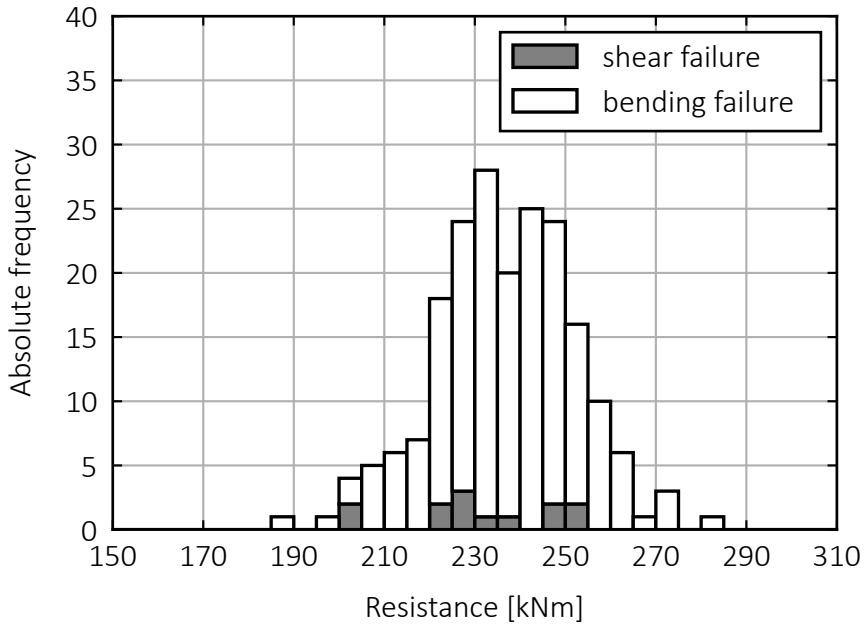

Figure 11. Histogram with stacked bars of the shear and the bending resistances for LTB of a beam of L x H x W = 8100 x 720 x 120 mm³ with scattering of geometrical and structural imperfections according to Sections 4.2 and 4.3; 200 computations.

5 Discussion and design proposal

For consistency with the in-plane buckling verification of glulam columns, the same equivalent bow imperfection should be chosen for the LTB design of glulam beams, namely $e_y = L/1000$ (prEN 1995-1-1, 2023). Otherwise, mechanical inconsistencies for the interaction of axial forces and bending moments cannot be avoided. For both, columns and beams, this value is supported by extensive measurements (*Ehlbeck* & *Blaß*, 1987), (*Töpler* & *Kuhlmann*, 2022b). To account for the influence of the remaining independently scattering geometrical and structural imperfections, the 95% quantile values of the twist imperfections given in Chapter 2 can be reduced by 50% and used as equivalent twist imperfections. This is illustrated by the comparison of T2O using these reduced imperfections with numerical results, see Figure 10. T2O calculations do not take into account twist imperfections at the supports. Therefore, the total twist imperfection at midspan was calculated as $0.5 \cdot (e_{\vartheta,\mathrm{mid},95} + e_{\vartheta,\mathrm{supp},95})$.
When comparing the ELM with the numerical results, see Figure 10, the influence of scattering imperfections is sufficiently accurately represented by the simplified approach in EN 1995-1-1 (2004). The new approach based on the Ayrton-Perry formulation in prEN 1995-1-1 (2023) yields similar load-bearing capacities. It should be noted that there is an additional small positive influence of the size effect represented by k_{red}, see Figure 10, and that the influence of scattering tensile strengths at small slendernesses far outweighs the influence of scattering imperfections.

Based on the investigations presented, equivalent imperfections for LTB design of glulam beams based on T2O calculations may be applied, as

$$e_{\mathrm{y,equi}} = e_{\mathrm{y}} \tag{4}$$

$$e_{\vartheta,\mathrm{mid,equi}} = 0.5 \cdot (e_{\vartheta,\mathrm{mid}} + e_{\vartheta,\mathrm{supp}}) \tag{5}$$

where $e_y = \frac{L}{1000}$, $e_{\vartheta,\mathrm{mid}} = \frac{L}{1500H}$, and $e_{\vartheta,\mathrm{supp}} = \frac{1}{150}$ or $\frac{1}{100}$ for low respectively high tolerances of the fork supports according to prEN 1995-1-1 (2023).
Assuming a pure bow imperfection of $e_y = L/400$ for LTB yields similar results to assuming imperfections according to Equations 4 and 5 and may be used for further simplification.

An approach for modelling both shear and bending failure of beams prone to LTB is presented. For the chosen cross-section and the loading by a constant bending moment $M_{y,I}$ in the numerical analyses, shear failure seems to be of minor importance. However, for more unfavourable loading conditions with high shear forces, such as in the LTB tests with 3-point bending, shear failure due to additional torsional moments at the supports is relevant. For the first time, prEN 1995-1-1 (2023) provides formulae for determining the torsional moments at the supports $M_{x,II}$ and might therefore lead to an increased awareness of this failure mode.

6 Summary and outlook

The results of 19 lateral torsional buckling tests on glulam beams made of GL 24h are described in this paper. The load-deformation behaviour was usually pronouncedly non-linear, see Figure 4. However, in 3 tests a bending failure occurred without prior lateral deflection of the beams. It is therefore possible that beams, despite their imperfection sensitivity, do not show a typical stability failure but a pure bending failure. Shear failure occurred in the slender test specimens and bending failure in the stockier ones, see Table 3 and Figures 6 and 7. Although this early shear failure reduced the stiffnesses and thus the load-bearing capacities by up to 20%, the design verifications according to EN 1995-1-1 (2004) and prEN 1995-1-1 (2023) are on the safe side, see Figure 5.

The FE model was validated with the test results and further developed to take into account both scattering geometrical imperfections and scattering structural imperfections across the board width for the determination of equivalent imperfections of imperfection-sensitive glulam beams. With an extensive data set of geometrical imperfections as input values (*Töpler* & *Kuhlmann*, 2022b), the model was used to investigate the influence of scattering geometrical and structural imperfections on the load-bearing capacity. Based on these results, see Figure 10, a proposal for equivalent imperfections for T2O calculations was developed and presented in Section 5. The current approach of the effective length method in EN 1995-1-1 represents the influence of these imperfections sufficiently accurately, see Figure 10.

For first studies of the influence of the shear failure on the lateral torsional buckling resistance the *Karlsruher Rechenmodell* (*Blaß* et al., 2008) was implemented and extended to include scattering of shear strengths (*Brüninghoff* & *Klapp*, 2005). The shear failure was of minor importance for the chosen cross-section and loading in the numerical analyses. However, for more unfavourable loading conditions with high shear forces, such as in the LTB tests with 3-point bending, shear failure due to additional torsional moments at the supports is relevant. This needs to be further investigated to ensure that early shear failure due to combined torsion and shear force does not lead to a reduction of the lateral torsional buckling resistance that has not yet been considered in design.

7 Acknowledgements

The research project is supported by the German Federal Ministry for Economic Affairs and Climate Action on the basis of a decision of the German Bundestag (IGF project no. 21285 N). This support is gratefully acknowledged. We thank the Forschungs- und Materialprüfanstalt (FMPA) of the Brandenburg University of Technology Cottbus-Senftenberg for conducting the experiments. Finally, we thank Schaffitzel Holzindustrie GmbH + Co. KG for providing the test specimens.

8 References

Aicher, S. & G. Dill-Langer (2000). “Basic considerations to rolling shear modulus in wooden boards”. In: *Otto-Graf-Journal* 11, pp. 157–165.

Blaß, H. J.; M. Frese; P. Glos; J. K. Denzler; P. Linsenmann & A. Ranta-Maunus (2008). *Zuverlässigkeit von Fichten-Brettschichtholz mit modifiziertem Aufbau*. Research report. University of Karlsruhe, Germany.

Brüninghoff, H. (1973). “Spannungen und Stabilität bei quergestützten Brettschichtholzträgern”. Dissertation. University of Karlsruhe, Germany.

Brüninghoff, H. & H. Klapp (2005). “Shear strength of glued laminated timber”. In: *CIB-W18*. 38-6-3, Karlsruhe, Germany.

Dahl, K. B. & K. A. Malo (2009). “Nonlinear shear properties of spruce softwood: experimental results”. In: *Wood Science and Technology* 43, pp. 539–558. DOI: https://doi.org/10.1007/s00226-009-0247-4.

Dahlblom, O.; S. Ormarsson & H. Petersson (1996). “Simulation of wood deformation processes in drying and other types of environmental loading”. In: *Annals of Forest Science* 53, pp. 857–866.

DIN EN 1995-1-1/NA (2013). *Nationaler Anhang – National festgelegte Parameter –Eurocode 5: Bemessung und Konstruktion von Holzbauten – Teil 1-1: Allgemeines – Allgemeine Regeln und Regeln für den Hochbau*. German Institute of Standardization (DIN), Berlin, Germany.

Ehlbeck, J. & H. J. Blaß (1987). *Zuverlässigkeit von Holzdruckstäben*. Research report. University of Karlsruhe, Germany.

Ehrhart, T. & R. Brandner (2018). “Rolling shear: Test configurations and properties of some European soft- and hardwood speciess”. In: *Engineering Structures* 172, pp. 554–572. DOI: https://doi.org/10.1016/j.engstruct.2018.05.118.

EN 14080 (2013). *Timber structures - Glued laminated timber and glued solid timber - Requirements*. European Committee for Standardization (CEN), Brussels, Belgium.

EN 1995-1-1 (2004). *Eurocode 5: Design of timber structures – Part 1-1: General – Common rules and rules for buildings*. European Committee for Standardization (CEN), Brussels, Belgium, with corrections and amendments + AC:2006 and A1:2008.

EN 408 (2010). *Structural Timber and Glued Laminated Timber – Determination of Some Physical and Mechanical Properties*. European Committee for Standardization (CEN), Brussels, Belgium, with corrections and amendments + A1:2012.

Frese, M. (2016). “Computergestützte Verfahren zur pragmatischen Beurteilung der Tragwiderstände von Brettschichtholz: Zusammenfassung exemplarischer Simulationsstudien”. Habilitation. Karlsruhe Institute of Technolgy. ISBN: 978-3-7315-0493-1.

Glos, P. (1978). “Zur Bestimmung des Festigkeitsverhaltens von Brettschichtholz bei Druckbeanspruchung aus Werkstoff- und Einwirkungskenngrößen”. Dissertation. Technical University of Munich, Germany.

Glos, P. & J. K. Denzler (2004). *Kalibrierung der charakteristischen Schubfestigkeitskennwerte für Vollholz in EN 338 entsprechend den Rahmenbedingungen der nationalen Sortiernorm*. Research report. Technical University of Munich, Germany.

Heimeshoff, B. (1986). "Berechnung und Ausführung von Holzbauwerken". In: *Ingenieur-Holzbau 86*. Leinfelden-Echterdingen, Germany.

Johansson, C.-J. (2003). "Grading of Timber with Respect to Mechanical Properties". In: *Timber Engineering*. Ed. by S. Thelandersson & H. J. Larsen. Chichester, England: Wiley. Chap. 10, pp. 23–43.

Kuhlmann, U. & J. Töpler (2021-2023). *Optimierung des Ersatzstabverfahrens für biegedrillknickgefährdete Bauteile aus Holz unter Momenten-Normalkraft-Belastung*. Research project, IGF No. 21285 N. Institute of Structural Design, University of Stuttgart, Germany.

Larsen, H. J. (1977). "Laterally Loaded Timber Columns, Tests and Theory". In: *CIB-W18*. 8-15-1, Brussels, Belgium.

prEN 1995-1-1 (2023). *Eurocode 5 — Design of timber structures — Part 1-1: General rules and rules for buildings*. CEN/TC 250/SC 5 N 1729. European Committee for Standardization (CEN): Brussels, Belgium.

Schilling, S.; P. Palma & A. Frangi (2021). "Probabilistic description of the mechanical properties of glued laminated timber made from softwood". In: *Proceedings of the 8th meeting of International Network on Timber Engineering Research (INTER)*. 54-12-4, online.

Spengler, R. (1986). "Festigkeitsverhalten von Brettelementen aus Fichte unter zweiachsiger Beanspruchung". In: *Baukonstruktion und Holzbau: Beiträge aus Lehre und Forschung. o. Prof. Dr.-Ing. Bodo Heimeshoff zum 60. Geburtstag*, pp. 125–157.

Töpler, J. (2024). "Load-bearing capacity of imperfection-sensitive timber members under combined bending and compression". unpublished. Dissertation. Institute of Structural Design, University of Stuttgart, Germany.

Töpler, J. & U. Kuhlmann (2022a). *Guidelines for a Finite Element Based Design of Timber Structures*. Mitteilung No. 2022-36X, Institute of Structural Design, University of Stuttgart, Germany. DOI: http://dx.doi.org/10.18419/opus-12769.

Töpler, J. & U. Kuhlmann (2022b). *Imperfektionsmessungen an stabilitätsgefährdeten Holzbauteilen*. Research report, DIBt P 52-5- 13.194-2048/19. Institute of Structural Design, University of Stuttgart, Germany. DOI: http://dx.doi.org/10.18419/opus-12578.

Töpler, J. & U. Kuhlmann (2022c). "In-plane buckling of beech LVL columns". In: *Proceedings of the 9th meeting of International Network on Timber Engineering Research (INTER)*. 55-2-1, Bad Aibling, Germany. DOI: http://dx.doi.org/10.18419/opus-12610.

Wilden, V.; B. Hoffmeister & M. Feldmann (2023). "Ein mechanisch konsistenter Ansatz für den Stabilitätsnachweis für Holztäger unter Druck und Biegung um die starke Achse". In: *Bautechnik* 100.Sonderheft Holzbau, pp. 19–30.